HIGH-DEGREE MODE FREQUENCIES: CHANGES WITH SOLAR CYCLE

M.C. Rabello-Soares[1], S.G. Korzennik[2], and J. Schou[1]

[1]*Stanford University, Stanford, CA, USA*
[2]*Harvard-Smithsonian Center for Astrophysics, Cambridge, MA, USA*

ABSTRACT

We present variations of high-degree ($100 \leq \ell \leq 900$) solar acoustic mode properties measured over most of solar cycle 23, estimated using global helioseismology analysis of full-disk observations. These observations were obtained with the Michelson Doppler Imager (MDI), one of the instruments on board the Solar and Heliospheric Observatory (SOHO) spacecraft.

We show here our latest results from a continuing effort to infer unbiased estimates of high-degree mode parameters. Known instrumental and observational effects that affect specifically high-degree modes were removed following the methodology described in detail in Korzennik, Rabello-Soares & Schou [6]. These new results allowed us to focus our attention on changes with solar activity.

Key words: Sun: helioseismology - Sun: Oscillations.

1. INTRODUCTION

The inclusion of high-degree modes (*i.e.*, ℓ up to 1000) has, for instance, the potential to improve dramatically the inference of the sound speed and the adiabatic exponent Γ_1 in the outermost 2 to 3% of the solar radius [8], a region of great interest. These high-ℓ modes also probe the second and first helium ionization zones and thus help constrain Γ_1, the adiabatic exponent.

Unfortunately, individual modes (n, ℓ, m) cannot be uniquely isolated using observations over the visible solar disk. Indeed, the spherical harmonics are not orthonormal over less than the full hemisphere, and thus the spatial filtering will not uniquely isolate a target (ℓ, m), resulting in what is referred to as spatial leakage.

At low and intermediate degree, these leaks are separated in the frequency domain from the target mode and individual modes can be identified and fitted. However, at high degree, the spatial leaks get closer in frequency (due to a smaller mode separation) and as the mode lifetimes get smaller, the resulting peaks get wider and eventually overlap. Hence at high-degree individual modes blend into ridges. The properties of the ridge (central frequency, amplitude, etc...) do not correspond to these of the underlying modes. This has so far hindered the estimation of unbiased mode parameters at high degrees.

To recover the actual mode characteristics, we need a very good model of the relative amplitude of all the modes that contribute to the ridge, aka the leakage matrix, which in turn requires a very good knowledge of the instrumental properties. The instrumental characteristics must therefore be very well understood and very precisely measured.

We present here our latest results from a continuing effort to estimate unbiased high-degree mode frequencies using full-disk data from the Michelson Doppler Imager (MDI), an instrument on-board the Solar and Heliospheric Observatory (SOHO). The methodology is based on the extensive analysis presented in Korzennik, Rabello-Soares & Schou [6] and will in turn be beneficial to MDI, GONG and eventually HMI.

These new results allowed us to focus our attention on changes with solar activity.

2. DATA ANALYSIS AND RIDGE MODELING

Full-disk dopplergrams, acquired by the MDI instrument while operating in its $4''$ resolution mode and known as the *Dynamics Program*, were used for this analysis. The MDI instrument is operated in this mode some 3 months every year, when the available telemetry bandwidth is large enough to transmit full-disk images.

We computed the spherical harmonic decomposition of the MDI images for every 10th ℓ between 100 and 900. From the resulting time-series of spherical harmonic coefficients we generated an averaged low resolution power spectrum to reduce realization noise while preserving enough resolution to adequately fit the ridge. Finally, we fitted the ridge (including its asymmetry) to determine the observed ridge parameters.

We also produced synthetic power spectra using a sophisticated model of the underlying modes that contribute to the ridge power distribution. We introduce all the known instrumental properties of MDI in our model. The ridge

model was generated with a frequency resolution similar to the observed power spectra for the same set of degrees. It was fitted using the same profile and methodology as the observed spectra.

The modes that actually leak into a given target mode spectrum (ℓ_0, m_0) with a significant amplitude and have to be taken into account in our ridge model are $|m - m_0| \leq 6$ and $|l - l_0| \leq D$, where $D = 12$ for $\ell \leq 600$ and increases up to 20 for $\ell = 1000$ [9].

We included in our model the distortion of the eigenfunctions by the solar differential rotation, as described in [10]. The resulting eigenfunctions can be expressed as a superposition of the undistorted ones. The coefficients in this superposition become negligible values when $|l - l_0| \geq D$, where $D = 10$ for $\ell \leq 400$ and increases up to 22 for $\ell = 1000$ [9].

To validate our procedure and our estimate of the resulting correction on the mode parameters, we introduce one instrumental effect at a time. Our goal is to be able to estimate the corrections needed to the ridge properties with an accuracy better than the precision of the corrected fitted values. If our model is correct and complete, our simulations should adequately estimate the frequency and splitting coefficient offsets between fitting ridges and fitting individual modes.

3. PROGRESS TOWARDS THE SOLUTION

3.1. Instrumental effects

As mentioned earlier, we need a very good model of the relative amplitude of all the individual modes that contribute to the ridge power distribution in order to recover unbiased mode parameters. Such a model requires that the instrumental characteristics be very well understood and very precisely measured.

The highly successful MDI instrument has been observing the Sun for over 10 years now and it is responsible for a great progress in our understanding of the Sun which we now know in considerable more details. However, there remains some instrumental effects that there are not well characterize and/or not taken into account in the data analysis.

In Korzennik, Rabello-Soares & Schou [6], we estimated the error budget for various contributions of instrumental effects to the required corrections for the mode central frequency and the a_1 splitting coefficient. These were compared to the observed fitting uncertainties. This error budget will be correct only if our model predictions are quantitatively correct. Therefore it is crucial to check the model by correcting the data one effect at a time.

We have implemented an improved spatial decomposition that now takes into account the following effects: uses the correct instantaneous image scale, includes the radial image distortion, the effect of a tilt of the CCD with respect to the optical axis, the effective P angle and a correction to the Carrington elements.

3.2. Image scale

The MDI instrument has been very stable over the years. Nonetheless, continuous exposure to solar radiation has increased the instrument front window absorption. This has resulted in a small increase of the instrument best focus. Besides, the annual temperature change of the front window due to the satellite orbit around the Sun, this effect has added an small annual variation to the best focus.

Image focusing on the MDI instrument consists of 9 possible focus positions (one focus step corresponding to approximately a third of a wave). The actual configuration in which the instrument was operating was changed over the years to best suit the science team needs, resulting in occasional abrupt jumps in the amount of the defocus of the images. For further details, see Bush et al. [3] and Korzennik, Rabello-Soares & Schou [6].

Variations in the amount of defocus have a direct influence in the image scale at the detector which, until now, were not taken into account in the spheric harmonic decomposition. The average scale change (at the solar limb) per focus block is 0.529 ± 0.002 pixels [7].

Figure 1 shows the effect on the mode central frequency and the a_1 frequency splitting when the best estimate of the time-varying image scale is taken into account, using Dynamics 1999 observations. The averaged image scale error for these data was 0.27%. Note that the effect on the central frequency for the f-modes (blue) is systematically larger than for p-modes (black). This confirms that the image scale correction has a strong effect on the horizontal component of the solar oscillations.

The improved central frequencies are now larger and the resulting change increases with frequency. For the p-modes the differences amount to 2.2 μHz around 2 mHz and increase linearly to reach 6.2 μHz at 4 mHz; above that frequency the trend gets steeper and reaches 12 μHz at 5.3 mHz. The improved a_1 splitting coefficients are larger than before by $\sim$1.5 nHz on average.

In Korzennik, Rabello-Soares & Schou [6] we modeled the effect of an error in the image scale. The prediction of this model is compared in Fig. 1 to the measured effect. Our model of this effect matches very well the observations in most cases. Except for some scatter, the frequency splittings are very close to the prediction.

For modes above 4 mHz, the central frequency changes were underestimated in our model. Note, however, that our model used a single image scale for the entire observing period, while the re-decomposition we carried out used our best estimate of the instantaneous image scale.

The observed ridge asymmetry differences are as large as

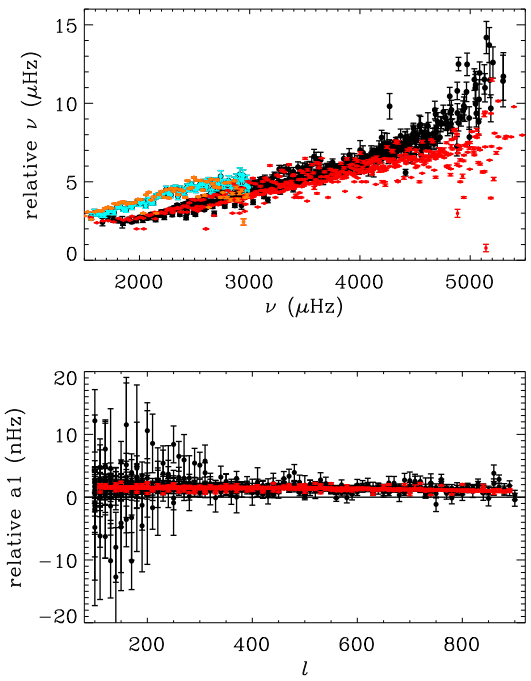

Figure 1. The observed frequency estimate changes, using Dynamics 1999 observations, when including the correct image scale in the spherical harmonic decomposition. P-modes are show in black, f-modes in blue. Our estimate of this effect, based on our model, are shown in red for p-modes and in orange for f-modes.

25%. Surprisingly, our model predicts much smaller differences (10% or less). Finally, the image scale correction seems to have no effect on the observed ridge width or amplitude.

3.3. Radial image distortion

The ray-trace model of MDI predicts a radial distortion which depends on the cubic distance from the CCD center. It causes the apparent solar radius to be larger by $\sim$0.8 pixels (17 μm).

We carried out a spherical harmonic decomposition that incorporates the radial distortion predicted by this ray-trace model. Figure 2 shows the effect on the mode central frequency. The effect predicted by our model is also shown for comparison.

The resulting central frequencies are now larger. The differences increases linearly with frequency: from $\sim$0.5 at 1.8 mHz to 2 μHz at 5 mHz. Our model of this effect compares very well with the observations. The improved a_1 splitting coefficients are also larger than before by $\sim$0.4 nHz on average.

The variation in the ridge linewidth is very small and increases linearly with frequency. The new linewidths are

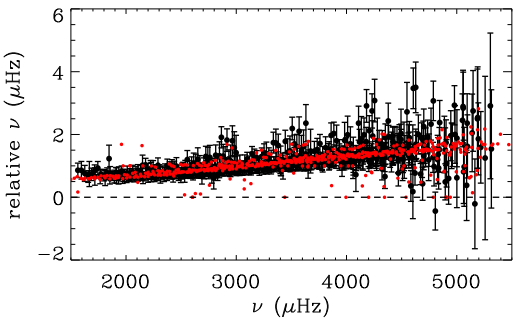

Figure 2. The observed frequency estimate changes, using Dynamics 2000 observations, when including the MDI image distortion in the spherical harmonic decomposition (black). Our estimate of this effect, based on our model, is shown in red.

0.1 μHz smaller at 1.8 mHz and 0.5 μHz larger at 5 mHz. The correction appears to have a small effect (1.5%) on the ridge amplitude only at low frequency ($\sim$2 mHz) and no effect on the observed asymmetry.

3.4. Non-radial distortion due to CCD tilt

Solar images as observed by MDI have a nearly elliptical shape with a difference between the semi-major axis and the semi-minor axis of about 0.6 pixels. This non-radial distortion is consistent with a small tilt of the CCD detector with respect to the focal plane. In Korzennik, Rabello-Soares & Schou [6], we estimated the non-radial distortion map resulting from this tilt. A tilt of $\sim 2^{\rm o}$ can account for the observed effect. Kuhn et al. [7] found a similar result (see Appendix A).

Surprisingly, the effect of our non-radial distortion model (assuming a $2.6^{\rm o}$ tilt) is very small in the mode parameters determination. The new central frequencies are larger by 0.1 μHz for $\ell \leq 400$. For higher ℓ, the difference increases slightly (0.4 μHz at $\ell = 900$). These are small variations but they are systematic and of the order of the fitting uncertainties (see budget tables in [6]).

The improved a_1 splitting coefficients are smaller than before by $\sim$0.1 nHz on average. On the other hand, the new a_2 is slightly larger by 0.015 nHz at $\ell = 200$ and difference decreases quadraticly with ℓ to reach nearly zero at $\ell = 900$.

The non-radial distortion correction seems to have no effect on the mode asymmetry or amplitude. The new linewidths are however 1% smaller.

3.5. Position angle P

The roll angle of the SOHO spacecraft is maintained such that the effective position angle, $P_{\rm eff}$, of the MDI images

should always be zero. However, a 0.2° difference has been measured (Cliff Toner - private communication).

No effect is seen in the mode parameters after including a correction of 0.2° in $P_{\rm eff}$. We do not see the effect on the a_1 splitting coefficient that was predicted in Korzennik, Rabello-Soares & Schou [6] using a slightly higher correction (0.25°). Note that the modeling of a P angle error in the leakage matrix is a tricky one, and thus not easily carried out accurately.

3.6. Carrington elements

Giles [5] showed that the standard values used for the two angles specifying the orientation of the solar rotation axis, known as the Carrington elements, are off by $\sim 0.1^{\rm o}$. This result was later confirmed by Beck & Giles [2]. This introduces a time dependent correction in the calculation of the P angle and the roll angle, B_0. This correction in the P angle will be on top of the one mentioned in the previous section. We found that this correction has no significant effect on the mode parameters.

3.7. Point spread function

As mentioned in section 3.2, the amount of defocus of the images changes with time. The largest variations happen when there is a change in the internal focus block resulting in a jump in the image defocus and, consequently, in the instrument point spread function.

The instrument PSF is incorporated more easily in the leakage matrix calculations than in the image spatial decomposition. Figure 3 shows the effect of including a Gaussian PSF (HWHM = 0.71 pixels) on the mode central frequency [6]. The difference in the results for f- and p_1-modes indicates a strong effect on the horizontal component of the solar oscillations. The differences are smaller than 0.15 μHz for the central frequencies and 0.08 nHz for the a_1 splitting coefficients.

The half-width at half maximum of the estimated azimuthally averaged PSF changes by ∼0.3 pixels over the whole Dynamics observations (1996 to 2005). Based on figure 3, this corresponds to a frequency variation of 0.07 μHz or less over all years.

The effect is likely to be nearly time independent. So we can start comparing results from different MDI Dynamics runs for $100 \leq \ell \leq 900$ and estimate changes with the solar cycle.

4. FREQUENCY CHANGES OVER THE SOLAR CYCLE

We have (re)processed 8 years of MDI Dynamics observations (see Table 1) for $100 \leq \ell \leq 900$ taking into account all known instrumental effects (except the PSF) in the image spatial decomposition.

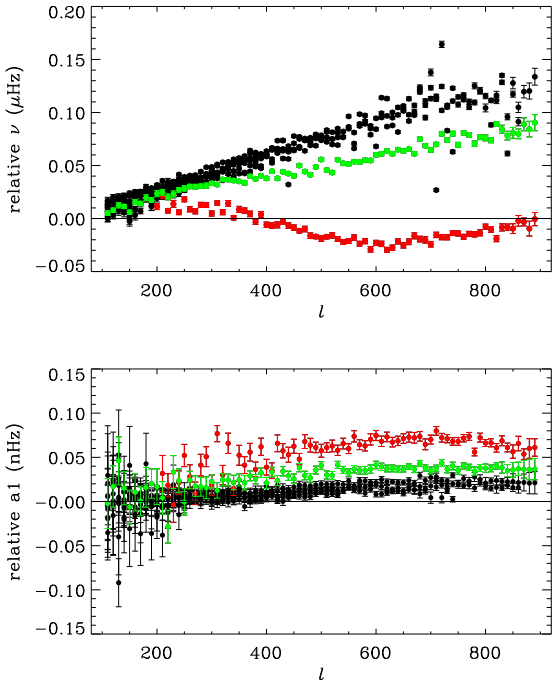

Figure 3. Effect of including a Gaussian PSF (HWHM = 0.71 pixels) in our ridge model on the central frequency (top) and a_1 splitting coefficients (bottom). The f-modes (in red) and the p_1-modes (in green) display a different behavior.

Table 1. Dynamics Observations Epochs and Relative Average MgII data.

Year	Starting Date month/day	Duration [days]	Mg II flux change with respect to 1996
1996	05/23	63	
1997	04/13	93	0.7
1998	01/09	92	3.9
1999	03/13	77	8.2
2000	05/27	45	14.3
2001	02/28	90	12.6
2003	10/18	38	10.6
2005	06/25	67	5.9

The data analyzed cover much of solar cycle 23. The first set, observed in 1996, corresponds to a period when the Sun's magnetic activity was nearly at its minimum, while for the one taken in 2000 the Sun was near maximum activity. The last set, taken in 2005, corresponds to a period of low solar magnetic activity when the Sun was approaching the solar minimum again. The average relative solar UV spectral irradiance (given by the MgII core-

to-wind ratio) with respect to 1996 for the eight epochs is shown in Table 1. We can thus study the changes of high-degree p-modes frequencies with the solar cycle by comparing results from our data sets during solar cycle 23.

We used the following three solar activity indexes in our study: solar UV spectral irradiance (MgII core-to-wing ratio data), solar radio 10.7 cm flux and solar sunspot number. They were obtained from the NOAA Solar Geophysical Data and the daily values were averaged over the observed period. The solar UV irradiance index shows the best correlation with the observed frequency shifts. Bhatnagar et al. [1] using GONG medium-degree modes ($2 \leq \ell \leq 150$) saw the same effect.

Figure 4 presents the frequency mean changes as a function of Mg II flux binned over ± 50 in ℓ. The frequency changes are computed with respect to 1996. We find a strong correlation of changes of the central frequency with the solar cycle 23 for all degrees. Arriving to this expected result gives us confidence in our analysis.

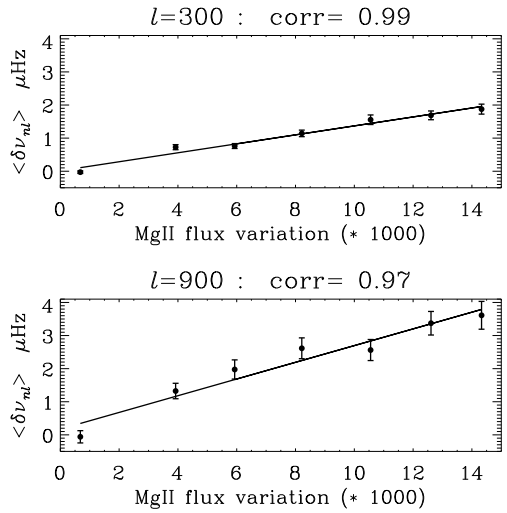

Figure 4. Mean changes in frequency as a function of Mg II flux for 2 different mean values of ℓ: 300 and 900. The linear Pearson correlation coefficient is 0.99 and 0.97 respectively. The error bars are the standard deviation of the mean in each bin.

Although this correlation is well known for some time now, its physical origin has been a matter of debate. The analysis of its behavior with frequency and degree will hopefully help us understanding it.

Figure 5 shows the frequency shift scaled by the mode inertia as a function of frequency binned over ± 50 μHz. Note the steady increase of the frequency shift with frequency for $\sim 2.2 \leq \nu \leq 4.6$ mHz, with a maximum at 4.6 mHz. The shifts seem to decrease above 4.6 mHz.

Figure 6 presents in more detail the frequency dependence of the frequency shift at high frequency. There is an intriguing sharp peak around 5 mHz during the declining phase of the cycle. For frequencies higher than 5.15 mHz, there is some evidence of negative shifts, specially during solar high activity (*i.e.*, 2000 and 2001).

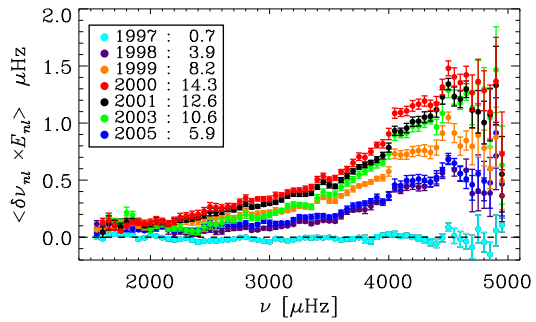

Figure 5. Changes in frequency multiplied by the mode inertia, shown binned, as a function of frequency. The error bars represent the scatter in the bin.

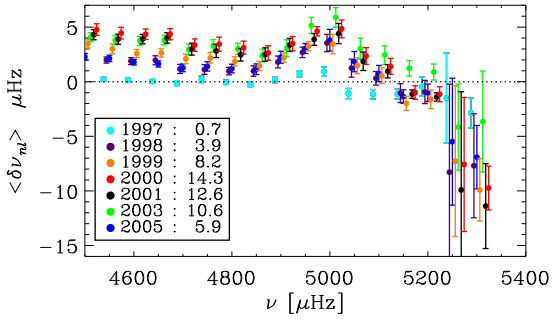

Figure 6. Mean changes in frequency (binned over ± 50 μHz) as a function of frequency.

In Fig. 7 we show the p- and f-modes separately. The observed different behavior of p- and f-modes suggests that different physical effects might be responsible for the changes in the mode frequencies with the solar cycle. The f-modes show a peak around 2.7 mHz. Its amplitude and width increase steady with activity. This is not seen for the p-modes. On the other hand, the p-modes frequency shifts show a minimum around 2 mHz at high activity and around 2.4 mHz at medium to low activity. Dziembowski & Goode [4] found a decrease in the shift for $\nu < 1.7$ mHz for the f-modes which when combined with our findings suggests a minimum at 1.7 mHz.

Figure 8 shows the frequency shift scaled by the mode inertia as a function of degree binned over ± 50 in ℓ. The dependence with the solar cycle is clearly visible. There is some evidence of variation with ℓ. We plotted selected years in separate plots to better visualize the variation with degree and separate the p-modes from the f-modes, see Figs. 9 and 10 respectively. A dependence on ℓ is more clearly seen for the f-modes. The frequency shift increases with ℓ for $\ell \leq 700$. This increase seems to become steeper with increased solar activity. There is a

peak around $\ell = 700$ that is visible for p-modes as well. Note that it is not present in 1997 when the solar activity was very low.

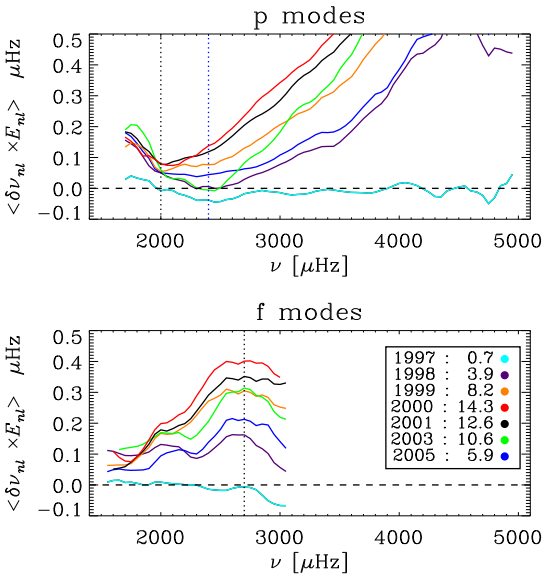

Figure 7. Same as figure 5, highlighting low frequency range for f- and p-modes separately.

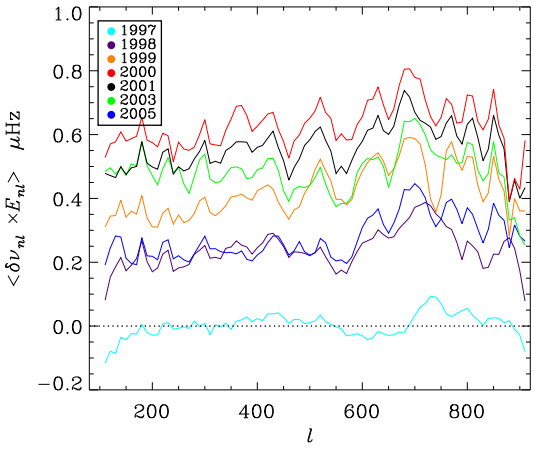

Figure 8. Changes in frequency, shown binned, as a function of degree. Note that, multiplying the shift by the mode inertia, get rid of most of the variation with ℓ.

5. CONCLUSION

The key improvement with respect to our previous work is the re-decomposition of the images onto spherical harmonic components incorporating our best knowledge of the MDI instrument on board SOHO.

As expected, by including these corrections in the spatial decomposition, the residual corrections that must be

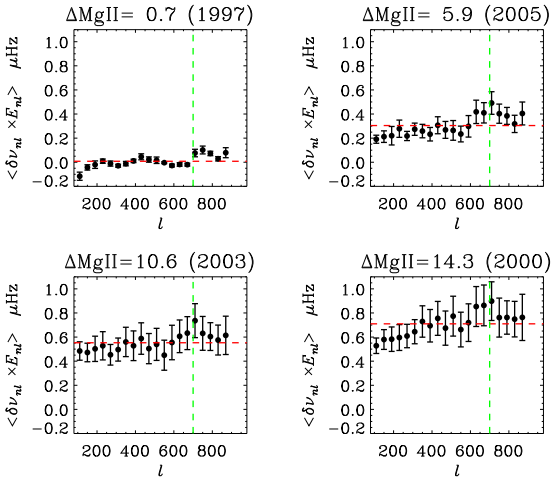

Figure 9. Normalized shifts for p-modes only.

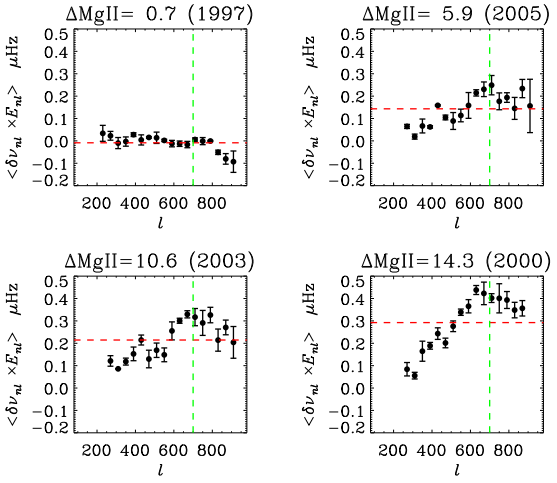

Figure 10. Normalized shifts for f-modes only.

applied to the ridge frequency are reduced, leading to a less biased frequency estimation; making possible the estimation of unbiased high-degree mode parameters using global helioseismology. This, in turn, allows us to focus our attention on the variation with the solar cycle of the mode parameters.

The well know correlation with the solar cycle is also seen at high degree. Our preliminary analysis of the frequency and degree dependence of the frequency shifts with the solar cycle suggest that the f-modes show a different behavior than the p-modes.

ACKNOWLEDGMENTS

The Solar Oscillations Investigation (SOI) involving MDI is supported by NASA grant NNG05GH14G at Stanford University. SOHO is a mission of international cooperation between ESA and NASA. SGK was supported by

NASA grant NNG05GD58G.

REFERENCES

[1] Bhatnagar, A., Jain, K., Thipathy, S.C., 1999, Ap. J. 512, 885

[2] Beck, J.G., Giles, P., 2005, Ap. J. 621, L153

[3] Bush R.I., Chu, K., Kuhn, J.R., 2001, AGU Fall Meeting, SH11B-0715

[4] Dziembowski, W.A., Goode, P.R., 2005, Ap. J. 625, 548

[5] Giles, P., 1999, PhD thesis, Stanford University, Stanford

[6] Korzennik, S.G., Rabello-Soares, M.C., Schou, J., 2004, Ap. J. 602, 481

[7] Kuhn, J.R. et al., 2004, ApJ 613, 1241

[8] Rabello-Soares, M.C., Basu, S., Christensen-Dalsgaard, J., Di Mauro, M.P., 2000, Sol. Phys. 193, 345

[9] Rabello-Soares, M. C., Korzennik, S.G., Schou, J. 2005, AGU Spring Meeting, SP11B-08

[10] Woodard, M.F., 1989, ApJ 347, 1176

A. COMPARISON OF NON-RADIAL DISTORTION ESTIMATION

Let us compare our model of the image non-radial distortion [6] with the one estimated by Kuhn et al. [7] and discuss the differences, in hope of finding a correct model of the image non-radial distortion. It should be noted that these models are based on different observational data.

It is believed that the CCD detector is tilted with respect to the focal plane which would explain the near elliptical shape of the solar limb observed by MDI. Both models assume that the detector is tilted by an amount α which results in a distortion that can be expressed as:

$$dx = -\frac{\alpha^2}{4}\,x + \frac{\alpha}{f}\,x\,y \qquad (1)$$

$$dy = \frac{\alpha^2}{4}\,y + \frac{\alpha}{f}\,y^2 - \frac{\alpha}{f}\,r_{\rm m}^2 \qquad (2)$$

where x and y are the detector coordinates, f the effective focal length and r_m the observed image mean radius. Although our equations have the same general form, there are differences in the parameters resulting in differences in the distortion maps (see Fig. 11).

The angle β defines the the orientation of the tilt and is measured from the detector's horizontal axis, x. We find $50^{\rm o} \leq \beta \leq 59^{\rm o}$ depending on the method we have used to estimate it. Kuhn et al. [7] found a similar value , namely $\beta = 55^{\rm o}$.

Depending on the method used, we find different values for α: $1.71^{\rm o} \leq \alpha \leq 2.6^{\rm o}$. Kuhn et al. [7] found $\alpha = 3.3^{\rm o}$, a surprisingly high value. To recover a nearly circular corrected undistorted solar limb, α ought to be $2.6^{\rm o}$ and $\beta \simeq 56^{\rm o}$.

The effective focal length f estimated by the ray-trace model of MDI is 13,000 pixels, the value we use in our model. Kuhn et al. [7] estimated $f = 14,006$ pixels.

In our model, the third term in the distortion in the y direction (*i.e.*, Eq. 2) is simply a translation that keeps the center of the image fixed and it is a constant:

$$\frac{\alpha}{f}\,r_{\rm m}^2$$

In [7], it is derived as proportional to r^2:

$$\frac{\alpha}{f}\,r^2$$

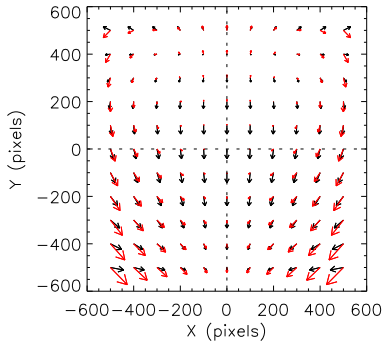

Figure 11. Distortion map given by our model in black [6] and Kuhn et al. [7] in red. For visualization purposes, the distortion has been exaggerated by a factor of 50.

We still have to understand the discrepancies between the distortion model parameters estimated using different observational methods. However, an approximate distortion map obtained using what we believe to be the best parameters will be an improvement compared to using no correction. This is what we did in section 3.4. Fortunately, the effect of a $2.6^{\rm o}$ CCD tilt on the mode parameters is small and we can safely extrapolate that the residual effect of the discrepancies in the distortion models can only be much smaller and most likely negligible.